Solid State Ionics 269 (2015) 57–61

Contents lists available at ScienceDirect

Solid State Ionics

journal homepage: www.elsevier.com/locate/ssi

The reaction of $Li_{6.5}La_3Zr_{1.5}Ta_{0.5}O_{12}$ with water

Yutao Li [a,b], Jian- Tao Han [b], Sven C. Vogel [c], Chang- An Wang [a,*]

[a] State Key Laboratory of New Ceramics and Fine Processing School of Materials Science and Engineering, Tsinghua University, Beijing 100084, PR China
[b] Materials Research Program and the Texas Materials Institute, ETC9.184, University of Texas at Austin, TX 78712, United States
[c] LANSCE-Lujan Center, Los Alamos National Laboratory, NM 87545, USA

ARTICLE INFO

Article history:
Received 7 July 2014
Received in revised form 3 November 2014
Accepted 8 November 2014
Available online 28 November 2014

Keywords:
Li-ion solid electrolyte
Garnet
Lithium-ion batteries
Ion exchange

ABSTRACT

The Li-ion conductor "$Li_{6.5}La_3Zr_{1.5}Ta_{0.5}O_{12}$" (LLZT) with garnet structure is prepared by solid-state reaction in an alumina crucible; its stability in water is investigated at room temperature. A Li^+/H^+ exchange is characterized by TGA, ^7Li and ^{27}Al MAS NMR, neutron diffraction, and TEM. In water, Li^+/H^+ exchange leads to a new garnet oxide "$Li_{6.5-x}H_xLa_3Zr_{1.5}Ta_{0.5}O_{12}$" (H-LLZT) with space group *Ia–3d*; the lattice parameter of H-LLZT is increased by the exchanged protons. Both LLZT and a grain boundary phase $LiAlO_2$ are unstable in water. The exchanged protons in H-LLZT displace Li from the octahedral sites bridging the 24*d* tetrahedral sites; they form a strong O–H bond that distorted the site. The amorphous phase $LiAlO_2$ in the grain boundary dissolves on exposure to water, which inhibits Li-ion transport across the grain boundary.

1. Introduction

Limitations of the flammable organic liquid-carbonate electrolytes of the Li-ion battery have stimulated interest in Li-ion solid electrolytes with high Li-ion conductivity at room temperature [1]. Li-rich garnet-related oxides have been studied extensively since Murugan et al. [2] reported in 2007 that the cubic garnet phase "$Li_7La_3Zr_2O_{12}$" exhibits a Li-ion conductivity $\sigma_{Li} > 10^{-4}$ S cm^{-1} at 25 °C and is chemically stable on contact with lithium metal. A variety of compositional variations have been investigated, including $Li_5La_3M_2O_{12}$ (M = Nb, Ta, Sb, Bi) [3–5], $Li_6ALa_3M_2O_{12}$ (A = Ca, Sr, Ba; M = Zr, Sn, Nb, Ta) [6–8] in order to vary the lattice constant and Li-ion population. In our lab, we found that Ta-doped garnet oxides $Li_{7-x}La_3Zr_{2-x}Ta_xO_{12}$ ($0.4 \le x \le 0.6$) showed a high Li-ion conductivity $\sigma_{Li} > 5 \times 10^{-4}$ S cm^{-1} at room temperature, and cyclic voltammetry also showed that the electrochemical potential of lithium is within the electrolyte window [9]. $Li_{7-x}La_3Zr_{1.5}Ta_{0.5}O_{12-\delta}$ sintered at 1000 °C by spark plasma sintering showed the highest Li-ion conductivity $\sigma_{Li} = 1.35 \times 10^{-3}$ S cm^{-1}, which is comparable to the commercial organic electrolyte [10]. These properties appeared to make Li-rich garnets good candidates for electrolytes in next generation Li-ion batteries, but deterioration of the surface of the pellets on exposure to air has prevented exploitation.

If the solid electrolyte is to separate a lithium anode and an aqueous, flow-through cathode, the solid electrolyte must be stable against water [1,11]. The instability with respect to water of garnet oxides, including tetragonal $Li_7La_3Sn_2O_{12}$ [12,13], cubic $Li_5La_3M_2O_{12}$ (M = Nb, Ta) [14] and $Li_{5+x}Ba_xLa_{3-x}Nb_2O_{12}$ (x = 0, 0.5, 1) [15], has been reported. Li^+/H^+ exchange was clearly observed, but the ionic distribution after the ion-exchange reaction was not clarified. Murugan *et al.* have reported that $Li_7La_3Zr_2O_{12}$ is stable in both air and moisture [2], so the stability of Zr- based garnet oxides may be different from that of other Li-rich garnet oxides. However, the Li-rich garnet electrolytes were contaminated by Al ions from high-temperature firing in an alumina crucible [16,17]. Al ions partially reside in the grain boundary to act as a sintering aid to improve the density of the ceramic and suppress Li loss at high temperature [7], and the phase in the grain boundary and its stability in water have not been investigated. Reaction with water of the grain-boundary phase will suppress intergrain Li^+ transport.

Here we have studied the instability of cubic $Li_{6.5}La_3Zr_{1.5}Ta_{0.5}O_{12}$ in water by using thermogravimetric analysis (TGA), ^7Li and ^{27}Al MAS NMR, TEM, and neutron diffraction measurements. The results show that both the bulk and grain boundary phases are unstable in water; Li ions on the octahedral sites of the bulk garnet phase are partially replaced by protons and the amorphous phase grain-boundary $LiAlO_2$ dissolves in water.

2. Experimental

A compound with chemical formula $Li_{6.5}La_3Zr_{1.5}Ta_{0.5}O_{12}$ (LLZT) was prepared by solid-state reaction of stoichiometric amounts of Li_2CO_3, La_2O_3 (heated at 900 °C for 12 h), ZrO_2 and Ta_2O_5. Excess Li_2CO_3 (20 wt.%) was added to compensate for the loss of lithium during annealing. The powders were ground and heated to 900 °C to decompose the metal salts, and then the powders were ground again, pressed into a pellet, and annealed at 1140 °C for 16 h in air while the pellet was covered with the same mother powder. The annealing was done in an alumina crucible.

* Corresponding author.
E-mail address: wangca@mail.tsinghua.edu.cn (C.-A. Wang).

http://dx.doi.org/10.1016/j.ssi.2014.11.010
0167-2738/

The prepared samples were crushed into powder for the ion-exchange reaction. The ion-exchange reaction was performed by placing 0.5 g of the garnet oxides in a flask containing 100 ml water of pH = 7. The experiments were carried out under constant stirring at room temperature. The duration of the exchange process was 48 h.

Thermogravimetric analysis was performed for ion-exchanged garnet in the temperature range of 40–800 °C in air. Powder X-ray diffraction (Philips PW1830, Cu Kα) was employed to monitor the phase formation in the 2-theta range 10 to 70° with a step size of 0.02°. The composition distribution of the elements was measured by inductively coupled plasma-optical emission spectroscopy (ICP-OES). Transmission electron microscopy (TEM) was performed in a Tecnai G2 20 microscope equipped with an EDX detector. The samples for TEM investigations were ground and ultrasonically dispersed in ethanol. One drop of the resulting suspension was placed on a TEM support.

Neutron diffraction experiments were conducted on the high-pressure preferred-orientation neutron diffractometer (HIPPO) at the Lujan Neutron Scattering Center, Los Alamos National Laboratory. Bulk samples were placed in a vanadium holder and time-of-flight data were collected under vacuum at room temperature. Neutrons were detected with 27 detector panels of ^{3}He detector tubes arranged on three rings with nominal diffraction angles of 40°, 90°, and 144°. The powder neutron-diffraction data were taken after ion-exchange of "$^7Li_{6.5}La_3Zr_{1.5}Ta_{0.5}O_{12}$" in water as described above.

^{7}Li and ^{27}Al NMR spectra recorded under MAS condition were obtained at room temperature with a B-VT 1000/SU07 unit adapted to an advance III 400 Bruker spectrometer. The frequency used for ^{7}Li was 155.50 MHz. Spectra were taken after a π/2 pulse irradiation and the interval between successive scans was chosen to avoid saturation effects (20–30 s); the spinning rate of the samples was 12 kHz and the number of accumulations was 4.

The sintered pellet was exchanged in water for 48 h at room temperature. Ionic conductivity was measured from 370 to 420 K with a Solar Impedance Analyzer (Model 1287); the applied frequency range was from 10^6 to 1 Hz with a 10 mV AC amplitude. Both parallel surfaces of the pellet were sputtered with Li-ion-blocking Au electrodes.

3. Results and discussion

The pH of the aqueous solution quickly reached about 10 after the LLZT powder was put into pH-7 water, and the pH stays at about 11 during the reaction, which is consistent with other reports on other garnet oxides [15]. This result clearly shows that protons from the water are consumed in an exchange reaction since the basic character of the oxide would not lose protons from bound surface water to pH-7 water. The protons enter into the garnet framework leaving hydroxide ions that are charge-compensated by Li ions from the garnet, which increases the pH of the solution.

Fig. 1 shows the XRD patterns of garnet powders after sintering and after ion-exchange. The ion-exchanged patterns are similar to that of $Li_5La_3Ta_2O_{12}$; the samples before and after ion exchange crystallize in the space group *Ia–3d*. A minor impurity phase $Al(OH)_3$ shows up after ion exchange because the amorphous grain-boundary phase containing Al is also unstable in water:

$$2LiAlO_2 + 3H_2O = 2Al(OH)_3 + Li_2O$$

The lattice parameter of H-LLZT (13.0123 Å) clearly increases after ion exchange owing to the replacement of symmetric Li – O bonds by asymmetric hydrogen O – H · · · O bonds [13], indicating the protons entered into the framework.

TGA curves in the temperature range from 40 to 800 °C of fresh garnet powders and powders after ion exchange are shown in Fig. 2. About 0.1 wt.% increase from room temperature to 400 °C for fresh garnet powders can be observed; the garnet powders may absorb some water or carbon dioxide in air. For the H-LLZT powders, two weight

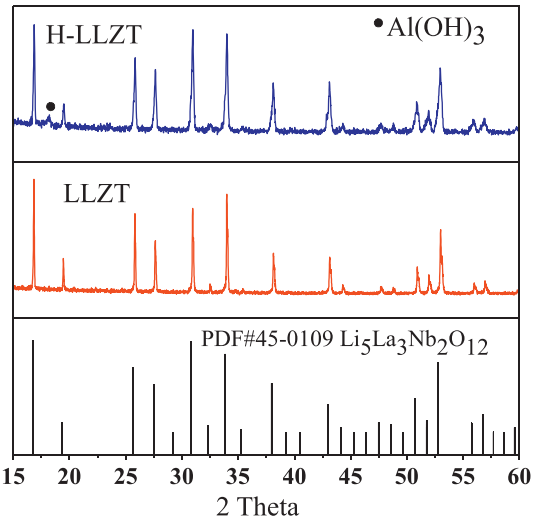

Fig. 1. Powder XRD results of LLZT and H-LLZT.

losses can be observed. The first one with 2 wt.% loss in the temperature range of 50–400 °C is ascribed to adsorbed water, while the second one with 5 wt.% loss in the temperature range of 400–600 °C indicates that the ion-exchanged phase dehydrates at high temperature. We have to note that Al ions were introduced into the garnet materials during the sintering process although there is no related peak in the XRD patterns. After ion exchange, the impurity phase $Al(OH)_3$ decomposes at high temperature to affect the TGA result. The composition of LLZT before and after ion exchange was confirmed by ICP (Table 1S). The content of both the Li and Al ions was reduced from LLZT after exposure to water, and about 21% Li ions were exchanged by protons.

The location of the Li atoms with X-ray diffraction is not feasible owing to the low X-ray scattering factor of Li; neutron diffraction was conducted on H-LLZT powder after the ion-exchange reaction to determine how the ionic distribution changed. The structure of cubic $Li_6BaLa_2Ta_2O_{12}$, in which the lithium is disordered with occupancies of 22% octahedral sites (48*g*), 21.8% displaced in octahedral sites (96*h*), and 67.4% tetrahedral sites (24*d*), was adopted as the initial structure model. (Note: The 48*g* positions are at the center of an octahedral site bridging equivalent 24*d* tetrahedral sites; the 96*h* positions are within the octahedral sites displaced toward an empty 24*d* site where an octahedron bridges an occupied and empty 24*d* site.). The three lithium and the oxygen sites, with their occupancies, were refined. This refinement led to a rather good agreement between the experimental and the calculated XRD patterns and to low reliability factors. The details of the

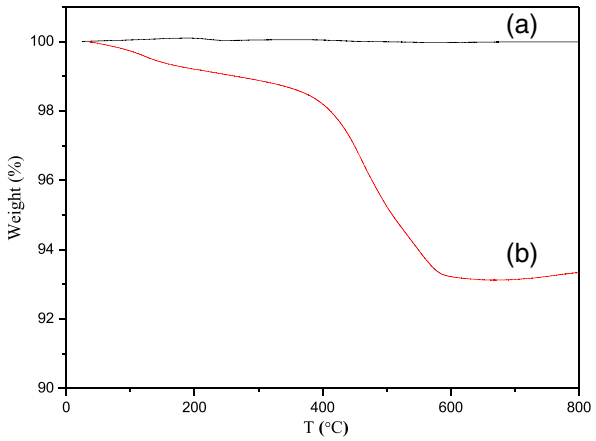

Fig. 2. TGA results of (a) LLZT and (b) H-LLZT.

Table 1
Structural parameters of "$^7Li_{6.5}La_3Zr_{1.5}Ta_{0.5}O_{12}$" garnet from Rietveld refinement of neutron diffraction data.

Atom	Site	x, y, z	Occupation	Uiso
Li1	24d	0.375, 0, 0.25	0.386(3)/0.388(8)[a]	0.011(3)
Li2	48g	0.125, 0.7912(17), 0.4588(17)	0.086(2)/0.288(7)[a]	0.024(6)
Li3	96h	0.1186(8), 0.2255(8), 0.4337(11)	0.169(1)/0.247(1)[a]	0.025(32)
La	24c	0.125, 0, 0.25	1	0.016(1)
Zr	16a	0, 0, 0	0.75	0.058(9)
Ta	16a	0, 0, 0	0.25	0.006(1)
O	96h	0.0999(4) 0.1958(9) 0.281(8)	0.995(8)	0.010(2)
Rp/Rwp/CHI^2	0.011/0.0088/10.98			

[a] Lithium occupancy of "$^7Li_{6.5}La_3Zr_{1.5}Ta_{0.5}O_{12}$".

Table 2
Interatomic distances (Å) in LLZT and H-LLZT.

	LLZT	H-LLZT
Li1 – O	1.918 (1) × 4	1.928(8) × 4
Li2 – O	2.009(8) × 2	1.544(6) × 2
	2.386(6) × 2	3.108(8) × 2
	2.413(5) × 2	3.135(8) × 2
Li3 – O	1.861(2) × 1	1.911(2) × 1
	2.051(8) × 1	2.035(9) × 1
	2.200(2) × 1	2.416(2) × 1
	2.237(9) × 1	2.437(3) × 1
	2.688(3) × 1	2.485(7) × 1
	2.754(1) × 1	2.570(4) × 1
Li1 – Li3	2.422(4)	2.319(1)
Zr – O	2.075(8) × 6	2.087(4) × 6
La – O	2.500 (5) × 4	2.514 (5) × 4
	2. 600(5) × 4	2. 620(1) × 4

data collection are shown in Table 1 and the fitted diffraction pattern is shown in Fig. 3. The lithium occupancy of "$^7Li_{6.5}La_3Zr_{1.5}Ta_{0.5}O_{12}$" before ion exchange is also listed in Table 1 for comparison.

The lithium occupancy of the tetrahedral 24*d* sites before and after ion exchange in garnet "$^7Li_{6.5}La_3Zr_{1.5}Ta_{0.5}O_{12}$" is almost the same while the lithium occupancy of the octahedral 48*g* sites and the displaced octahedral 96*h* sites after ion exchange is reduced by 8.6% and 16.9%, respectively; only the Li ions on octahedral sites are exchanged by the protons in water. The formula of "$^7Li_{6.5}La_3Zr_{1.5}Ta_{0.5}O_{12}$" after the ion-exchange reaction, as determined by neutron diffraction, is "$^7Li_{3.72}H_{3.28}La_3Zr_{1.5}Ta_{0.5}O_{12}$"; the protons are not visible, and about 27 mol.% of Li ions are lost compared to the ICP result before ion exchange. The bond distances of "$Li_{6.5}La_3Zr_{1.5}Ta_{0.5}O_{12}$" are listed in Table 2, two Li2 – O bond distances after ion exchange (1.545 Å) are much shorter than the normal bond distance (2.009 Å), while the other Li2 – O bond distances increase. After Li^+/H^+ exchange, the Li – O octahedra become more distorted; these sites are almost empty of Li ions, so the distortion implies that the protons occupy these sites; the Li3 – O distance does not change too much, and the Li ions seem to be more stable on octahedral 96*h* sites, but the shorter Li1 – Li3 interatmoic distance (2.319 Å) in "$^7Li_{6.5-x}H_xLa_3Zr_{1.5}Ta_{0.5}O_{12}$" than that in "$^7Li_{6.5}La_3Zr_{1.5}Ta_{0.5}O_{12}$" (2.422 Å) shows that the protons change the magnitude of the 96*h* displacement.

The extent of Li^+/H^+ exchange depends on the population of Li in octahedral interstitial sites of the garnet framework $B_3C_2O_{12}$. A $Li_xB_3C_2O_{12}$ garnet with $x \le 3$ contains Li only in the tetrahedral sites 24*d* and is stable in water [13]. Truong and Thangadurai [15] have reported that the higher Li-ion population of garnet-type $Li_{5+x}Ba_xLa_{3-x}Nb_2O_{12}$ ($x = 0, 0.5, 1$) leads to a smaller ion exchange,

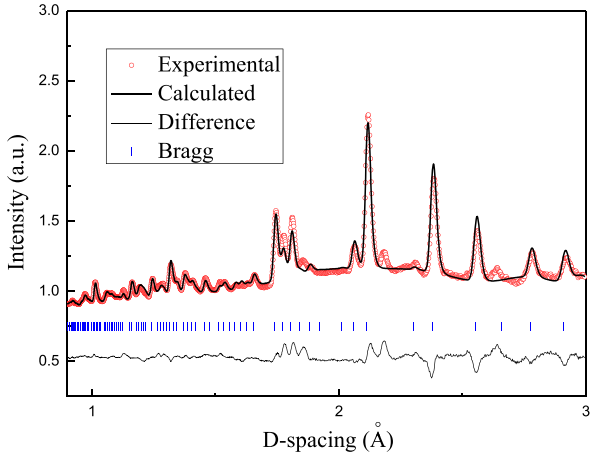

Fig. 3. Observed, calculated, and difference patterns for the Rietveld refinement from neutron diffraction of H-LLZT. The short vertical lines below the profiles mark the peak positions of all possible Bragg reflections.

but they did not identify which Li were being ion-exchanged; they reported a neutron-powder-diffraction (NPD) study on $L_{5-x}D_xNb_2O_{12}$ at 4 K in deuterated water [14]. With 5 Li atoms, occupied octahedral sites 96*h*/48*g* are in the ratio 20/9, and they reported only observing D exchange into the 96*h* sites. From TGA data, they obtained 2.4 Li per formula unit were exchanged by protons. The NPD data showed the deuteron formed one short D – O bond of 0.969(2)Å. We have tested the stability of the cubic garnets $Li_{7-x}La_3Zr_{2-x}Ta_xO_{12}$ with $x = 0$ and $x = 0.5$ by TGA in water and NPD in deuterated water at room temperature; both samples were found to exchange H^+ for Li^+; the details of the refinement and the diffraction pattern of $^7Li_{7-x}D_xLa_3Zr_2O_{12}$ are shown in Table 3S and Fig. 1S. The Li – O octahedra were distorted and the longer Li1 – Li3 interatomic distance in the 96*h* sites decreased from 2.439 Å to 2.388 Å in the $x = 0$ samples $Li_{7-x}D_xLa_3Zr_2O_{12}$ (Table 2S). We failed to identify the relative position of the deuterons in the $x = 0$ $Li_7La_3Zr_2O_{12}$. The La – O and Zr – O bond lengths in exchanged garnets were changed little.

^7Li MAS NMR was used to probe the Li dynamics in LLZT and H-LLZT. In Fig. 4, the ^7Li NMR spectrum displays a central transition ($-1/2 \rightarrow 1/2$) resonance around 0 ppm, and the smaller line width at half-maximum height (280 Hz) in LLZT indicates a higher Li-ion mobility in LLZT than that in H-LLZT (700 Hz). The two-component NMR line was represented by a composite of a broad (Gaussian) and a narrow (Lorentzian) component, which can be assigned to ^7Li populations with higher and lower ion mobility. The area fraction (A_f) of the narrow contribution, representing fast Li ions in LLZT and H-LLZT, amounts to approximately 84% and 72%, respectively.

The cubic garnet phase can be stabilized by replacement of $3Li^+$ with Al^{3+} in "$Li_7La_3Zr_2O_{12}$" [16]; the Al^{3+} comes from the alumina crucible. In our previous work, we found that the Al partially resided in the grain boundary as a sintering aid to improve the density of the ceramic and suppress Li loss at high temperature in garnets $Li_{7-x}La_3Zr_{2-x}Ta_xO_{12}$ ($0 \le x \le 1$). The Al^{3+} content in LLZT depends on the content of excess lithium used to compensate lithium loss at high temperatures (Table 1S). The compositions of LLZT with different amounts of excess lithium, confirmed by ICP are listed in Table S1; more Al ions are introduced into the garnet LLZT as the lithium content increases. LLZT with good mechanical and electrical performance can be obtained if about 20 wt.% Li_2CO_3 is added into the starting materials, and less or more lithium will increase the grain boundary resistance.

The ^{27}Al MAS NMR line around 74 ppm (Fig. 4.) confirms the existence of $LiAlO_2$. The garnet LLZT was coated by an amorphous phase (Fig. 5(a)), and the molar ratio of Al to O of the amorphous phase confirmed by EDX is close to 2:1 (Fig. 5(c)). The ^{27}Al MAS NMR spectra of LLZT and H-LLZT are shown in Fig. 4. Three main Al signals can be distinguished. The signal at 11 ppm was assigned to $LaAlO_3$, which is not observed in the XRD pattern [16]; the ^{27}Al NMR line at 74 ppm results from the grain-boundary phase $LiAlO_2$, and the line at 60 ppm is usually

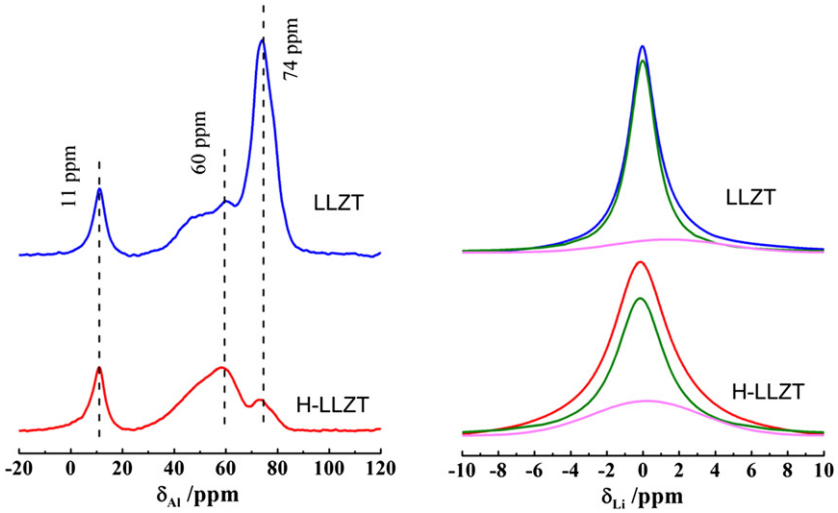

Fig. 4. ^{27}Al and ^{7}Li MAS NMR spectra of LLZT and H-LLZT at room temperature, the line shape of ^{7}Li is fit as a sum of broad and narrow component associated with slow and fast lithium ion domains.

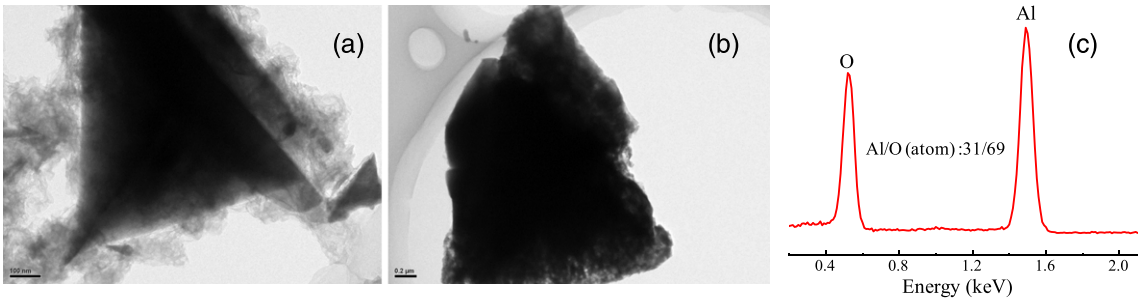

Fig. 5. (a) TEM image of LLZT. (b) TEM image of H-LLZT. (c) EDX result of amorphous phase in grain boundary.

assigned to aluminum in 4-fold coordination with oxygen, which may reside in an amorphous grain-boundary phase. Al ions may replace lithium ions on tetrahedral 24*d* sites with a corresponding NMR signal at 64 ppm [18], which is covered by the NMR line at 60 ppm. After ion exchange, almost half of the Al ions are removed (Table 1S); the TEM result (Fig. 5(b)) also shows that H^+ not only reacts with $LiAlO_2$ in the grain boundary, but also with the bulk garnet LLZT. The lower intensity of ^{27}Al NMR signal at 74 ppm in LLZT indicates the instability of the grain-boundary $LiAlO_2$ in water. A minor phase $Al(OH)_3$ also existed after ion exchange.

An impedance spectrum of H-LLZT is exhibited in Fig. 6(a). The appearance of a low-frequency tail in the case of ionically blocking electrodes is an indication that the conductivity is ionic in nature. A clear semicircle was observed in the high-frequency region, but it did not extrapolate to the origin; the distance from zero to the intercept of the linear tail with the real axis was assigned to the total conductivity. The impedance plot could be resolved into bulk, grain-boundary, and electrode resistances. The total (bulk + grain-boundary) conductivity of the garnet H-LLZT at 25 °C is 3.2×10^{-5} S cm^{-1}, which is at least one order of magnitude lower than that of the sintered pellet before the ion-exchange reaction [9]. The compactness of the as-synthesized garnets affects the ion-exchange rate of the pellets, which make the ion-exchange reaction different between the LLZT powders and pellets.

Fig. 6(b) shows the lithium-ion conductivity as a function of 1000/T for the ion-exchanged H-LLZT. The temperature dependence of the conductivity can be expressed by the Arrhenius equation. The activation

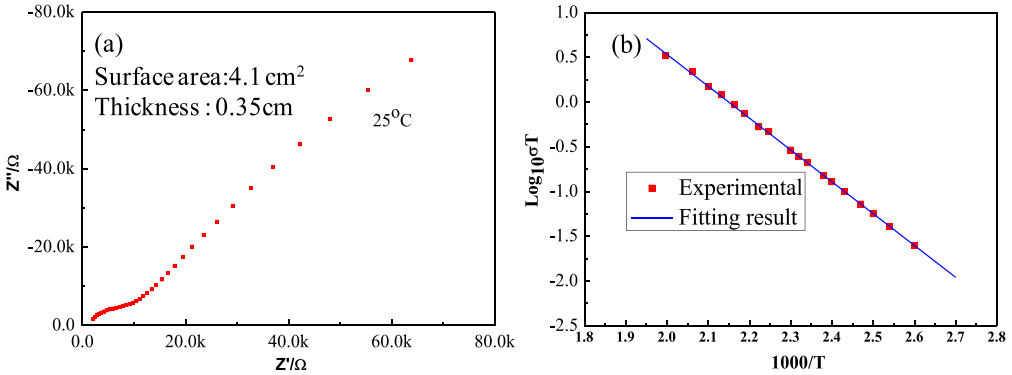

Fig. 6. (a) Impedance plot (10 Hz–1 MHz) of H-LLZT measured in air. (b) Temperature dependence of lithium conductivity of H-LLZT.

energy of H-LLZT was estimated to be $E_a = 0.38$ eV from the slope of the logσT versus 1000/T plot in the temperature range of 100–250 °C. The activation energy of the ion-exchanged H-LLZT pellets is higher than that of LLZT (0.30 eV), but this change primarily reflects an important change in the grain-boundary contribution.

4. Conclusions

In this paper, we have investigated the Li^+/H^+ ion exchange of garnet-related $Li_{6.5}La_3Zr_{1.5}Ta_{0.5}O_{12}$ in water at room temperature. A new garnet oxide $Li_{6.5-x}H_xLa_3Zr_{1.5}Ta_{0.5}O_{12}$ was obtained after Li^+/H^+ exchange. $Li_{6.5-x}H_xLa_3Zr_{1.5}Ta_{0.5}O_{12}$ crystallizes in the space group *Ia–3d* and its lattice parameter was increased by the exchange of protons for Li. Both the bulk and grain-boundary phase of LLZT are unstable in water. The exchanged protons distort the Li–O octahedra and reduce the occupancy of Li on the octahedral sites of the bulk phase, especially that of the 48*g* sites, and the Li ions in $Li_{6.5-x}H_xLa_3Zr_{1.5}Ta_{0.5}O_{12}$ become less mobile. The amorphous phase $LiAlO_2$ in the grain boundary is dissolved after ion exchange, which inhibits the lithium transport in the grain boundary. The total (bulk + grain-boundary) conductivities of the garnets $Li_{6.5-x}H_xLa_3Zr_{1.5}Ta_{0.5}O_{12}$ at 25 °C are 3.2×10^{-5} S cm^{-1} with an activation energy of 0.38 eV. The lowering of σ_{Li} and increase in E_a after reaction with water could be attributed primarily to a greater grain-boundary resistance.

Acknowledgment

This work was supported by the National Natural Science Foundation of China (NSFC-No. 51221291).

Appendix A. Supplementary data

Supplementary data to this article can be found online at http://dx.doi.org/10.1016/j.ssi.2014.11.010.

References

[1] J.B. Goodenough, Y. Kim, Chem. Mater. 22 (3) (2009) 587.
[2] R. Murugan, V. Thangadurai, W. Weppner, Angew. Chem. Int. Ed. 46 (41) (2007) 7778.
[3] V. Thangadurai, H. Kaack, W.J.F. Weppner, J. Am. Ceram. Soc. 86 (3) (2003) 437.
[4] Ramaswamy Murugan, Werner Weppner, Peter Schmid-Beurmann, Venkataraman Thangadurai, Mater. Sci. Eng. B Solid State Mater. Adv. Technol. 143 (2007) 14.
[5] May Nyman, Todd M. Alam, Sarah K. McIntyre, Grant C. Bleier, et al., Chem. Mater. 22 (19) (2010) 5401.
[6] Hui Xie, Yutao Li, Jian-tao Han, et al., J. Electrochem. Soc. 159 (8) (2012) 1148.
[7] Yutao Li, Chang-an Wang, Hui Xie, et al., Electrochem. Commun. 13 (12) (2011) 1289.
[8] V. Thangadurai, W. Weppner, Adv. Funct. Mater. 15 (2005) 107.
[9] Yutao Li, Jian-tao Han, Chang-an Wang, et al., J. Mater. Chem. 22 (30) (2012) 15357.
[10] Seung-Wook Baek, Jae-Myung Lee, Tae Young Kim, et al., J. Power Sources 249 (2014) 197.
[11] Yuhao Lu, J.B. Goodenough, Y. Kim, J. Am. Chem. Soc. 133 (15) (2011) 5756.
[12] Cyrille Galven, Jean-Louis Fourquet, Marie-Pierre Crosnier-Lopez, et al., Chem. Mater. 23 (7) (2011) 1892.
[13] Cyrille Galven, Jens Dittmer, Emmanuelle Suard, et al., Chem. Mater. 24 (17) (2012) 3335.
[14] L. Truong, Matthew Howard, Oliver Clemens, et al., J. Mater. Chem. A 1 (43) (2013) 13469.
[15] L. Truong, V. Thangadurai, Chem. Mater. 23 (17) (2011) 3970.
[16] Charles A. Geiger, Evgeny Alekseev, Biljana Lazic, et al., Inorg. Chem. 50 (3) (2010) 1089.
[17] H. Buschmann, Henrik Buschmann, Janis Dölle, et al., Phys. Chem. Chem. Phys. 13 (43) (2011) 19378.
[18] Andre Düvel, Alexander Kuhn, Lars Robben, et al., J. Phys. Chem. C 116 (29) (2012) 15192.